

Connecting the macroscopic phase of a Bardeen-Cooper-Schrieffer condensate to static electric fields

Federico Paolucci,^{1,2,3,*} Francesco Vischi,^{2,4,3} Giorgio De Simoni,²

Claudio Guarcello,² Paolo Solinas,⁵ and Francesco Giazotto^{2,†}

¹ INFN Sezione di Pisa, Largo Bruno Pontecorvo, 3, I-56127 Pisa, Italy

² NEST, Istituto Nanoscienze-CNR and Scuola Normale Superiore, I-56127 Pisa, Italy

³These authors equally contributed to this work.

⁴ Dipartimento di Fisica dell'Università di Pisa, Largo Pontecorvo 3, I-56127 Pisa, Italy

⁵ SPIN-CNR, Via Dodecaneso 33, I-16146 Genova, Italy

The possibility of tuning the properties of Bardeen-Cooper-Schrieffer metallic superconductors via conventional gating has been excluded for almost a century. Surprisingly, strong static electric fields have been recently shown to modulate the supercurrent down to full suppression and even to induce a superconductor-to-normal phase transition in metallic wires [1] and Josephson junctions (JJs) [2–4] without affecting their normal-state behavior. Yet, these results did not find a microscopic theoretical explanation so far [5]. Here, we lay down a fundamental brick for both the insight and the technological application of this unorthodox field-effect by realizing a titanium-based monolithic superconducting quantum interference device (SQUID) which can be tuned by applying a gate bias to both JJs independently. We first show modulation of the amplitude and the position of the interference pattern of the switching current (I_S) by acting with an external electric field on a *single* junction of the interferometer. Notably, this phenomenology cannot be explained by a simple squeezing of the critical current of the junction induced by the electric field [6]. Consequently, a local electric field acts on a global scale influencing the properties of both JJs. Since the superconducting phases of the two JJs are non-locally connected by fluxoid quantization, we deduce that the electric field must act both on the critical current amplitude and *couple* to the superconducting phase across the single junction. The overall interferometer phase can shift from -0.4π to 0.2π depending on the used gate electrode and on the strength of the gate bias. Furthermore, the effect persists up to $\sim 80\%$ of the superconducting critical temperature. Fully-metallic field-effect controllable Josephson interferometers could lay the first stone of novel superconducting architectures suitable for classical [7, 8] and quantum [9–12] computing, and for ultrasensitive tunable magnetometry [13, 14].

Figure 1-a shows a typical field-effect controllable metallic Josephson interferometer. The monolithic de-

SQUID is realized in the form of a 30-nm-thick Ti superconducting loop interrupted by two 150-nm-long and 150-nm-wide nano-constrictions (Dayem-bridges), that we label as L for left and R for right. Corresponding to each constriction a side electrode (V_L and V_R , at a distance of about 30 nm and 50 nm, respectively) allows to independently control the switching current of the JJ (I_L and I_R) via an electrostatic field [1–3]. The details of the simple single-step fabrication process can be found in the Methods.

We start the basic investigation of our interferometer by measuring its resistance R versus temperature T characteristic shown in Fig. 1-b. In particular, a critical temperature $T_C \simeq 420\text{mK}$ and a normal-state resistance $R_N \simeq 550\Omega$ are recorded. To study the current-flux behavior of the SQUID, we measured the voltage versus current characteristics for $\Phi \simeq 0$ (orange) and $\Phi \simeq \Phi_0/2$ (blue), where $\Phi_0 \simeq 2 \times 10^{-15}$ Wb is the flux quantum, at $T = 150$ mK (see Fig. 1-c). Denoting with $I_S(\Phi)$ and $I_{S,ave}$ the switching current as a function of the magnetic flux and the average current, respectively, a modulation visibility $\Delta I_S/I_{S,ave} \simeq 11\%$ is observed, where $\Delta I_S = I_S(0) - I_S(\Phi_0/2)$.

The characteristic triangular magnetic-flux patterns [15, 16] of both positive (blue) and negative (orange) branch of the switching current obtained at $T = 50$ mK are represented in Fig. 1-d. In order to extract the basic parameters of the interferometer we developed a theoretical model based on the resistively and capacitively shunted junction (RCSJ) formalism (see Methods for further details). The black lines in Fig. 1-d are obtained by considering a working temperature of 50mK and the presence of thermal fluctuations on both JJs (I_L^h and I_R^h). We deduced the screening parameter, $\beta \simeq 32$, accounting for the multiple value of I_S for certain values of magnetic flux [17], and a small asymmetry in the critical current of the two junctions ($I_{C,L} \simeq 13.6\mu\text{A}$ and $I_{C,R} \simeq 13.3\mu\text{A}$, respectively) causing the limited offset of $I_S(\Phi)$ along the external magnetic flux axis ($\simeq 0.05\Phi_0$).

To ensure independent field-effect control of a single JJ, the intensity of the electric field generated through the left (right) gate electrode at the surface of the right (left) Dayem bridge has to be negligible. To this end, we fabricated the junctions separated by roughly $8 \mu\text{m}$ (see

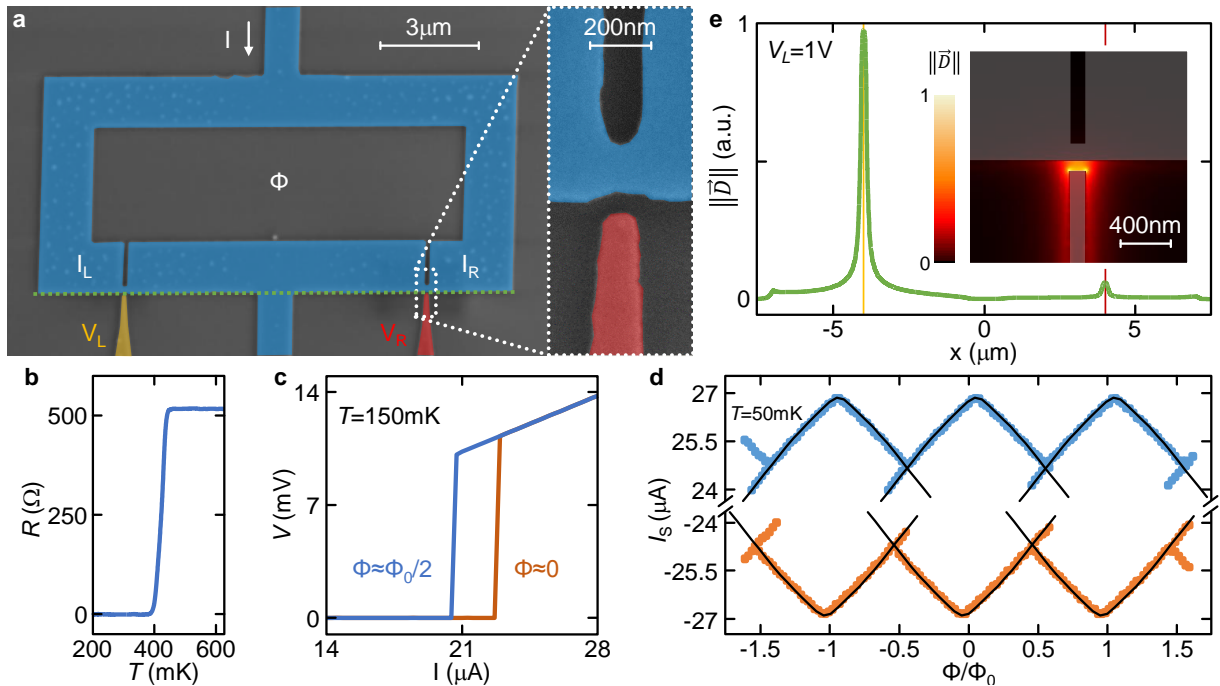


FIG. 1: **Interferometer layout and basic characterization.** **a** False-color electron micrograph of a typical all-metallic field-effect controllable Josephson interferometer. The core of the SQUID is represented in blue whereas the left side gate (V_L) in yellow and the right side gate (V_R) in red. Φ denotes the magnetic flux piercing the loop while I is the current flowing through the interferometer. The inset shows a blow-up of the right gate-tunable Josephson junction. **b** Four-probe resistance R versus temperature T characteristic of the device. **c** Individual voltage V versus current I traces measured at $T = 150$ mK for $\Phi \approx 0$ (orange) and $\Phi \approx \Phi_0/2$ (blue). **d** Positive (blue squares) and negative (orange squares) switching currents I_S of the SQUID measured at $T = 50$ mK. The black lines represent the theoretical prediction for a Dayem-bridge-based SQUID calculated within the RCSJ formalism (see Methods for further details). The resulting error bars are smaller than the line dimension. **e** Finite element calculation of the norm of the electric displacement field $\|\vec{D}\|$ calculated along the green dotted line in **a** in the geometry of our SQUIDs for $V_L = 1$ V. The yellow and red vertical lines indicate the position of the left and right JJ, respectively. The inset shows a 2-dimensional simulation of the distribution of $\|\vec{D}\|$ around the left constriction for $V_L = 1$ V.

Fig. 1-a) [1]. As a check, we performed a finite element simulation of the distribution of the electric displacement field \vec{D} at $V_L = 1$ V for the same geometry of our devices (see Methods). Figure 1-e shows that the resulting $\|\vec{D}\|$ is suppressed by about a factor of 20 at the right JJ so that the effect of V_L on I_R can be considered negligible. Moreover, the electric field generated by the left gate electrode is mostly directed on the constriction area (see the inset of Fig. 1-e), and it can affect the arms of the SQUID for a very small length compared to the total SQUID perimeter (i.e., for a few percent).

To investigate the impact of the gate bias on the SQUID switching current characteristic, we measured $I_S(\Phi)$ for different values of gate voltage independently applied to both the left (V_L) and right (V_R) gate electrode. Figures 2-a and b show the magnetic modulation patterns of the positive and negative branch of the switching current for different positive values of V_L measured at $T = 50$ mK. The data highlight several interesting gate-dependent features. First, the maximum switch-

ing current $I_{S,max}$ is suppressed by increasing gate voltage, and it shows a similar reduction for positive and negative current bias. Second, $I_{S,max}$ shifts towards lower (higher) magnetic flux values for the positive (negative) branch of the switching current. Third, the experimental error bars of I_S are different in the first and second half of the oscillation period with the magnetic flux. They grow for the first half period of the switching current, whereas they remain almost constant for the second one.

Importantly, field-effect is almost symmetric in the polarity of V_L (see Fig. 2-c), as reported for the reduction of I_S in metallic wires [1] and Dayem-bridge JJs [2, 3]. As a consequence, any charge accumulation or depletion seem to be excluded since they would provide an opposite effect on the magnitude of the switching current.

In full agreement with the data obtained for V_L , by applying a bias V_R to the right gate electrode yields suppression of the maximum switching current (see Fig. 2-d). Yet, the magnetic modulation patterns shift towards higher values of the magnetic flux and the larger current

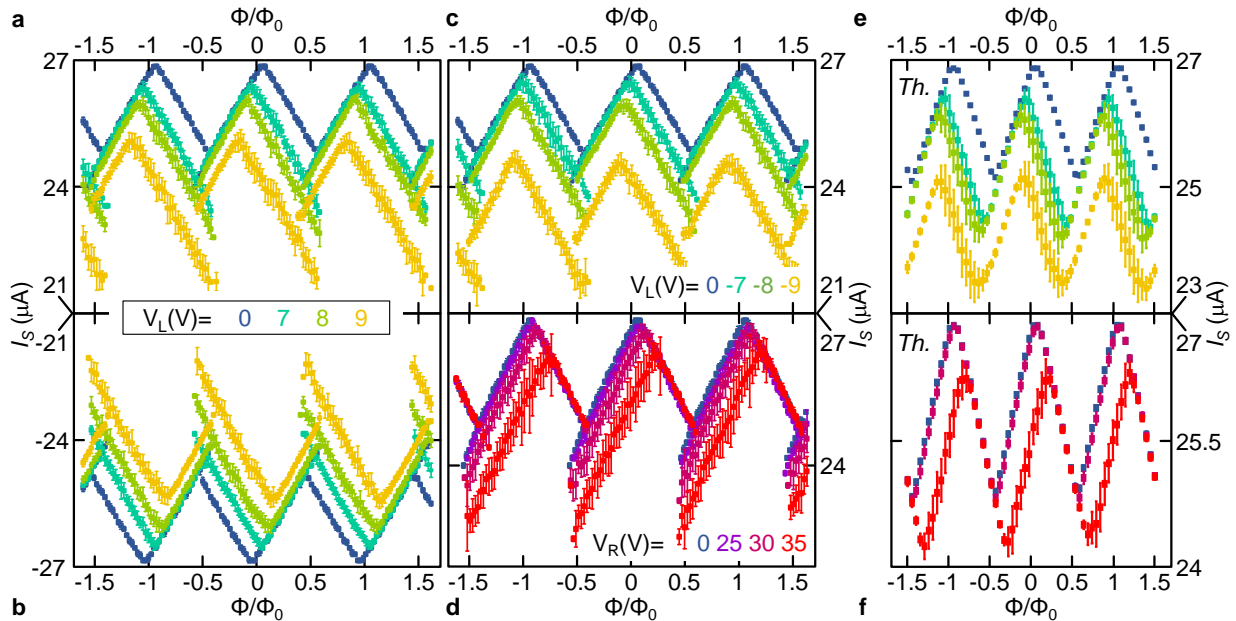


FIG. 2: **Electric field-dependent magnetic modulations: experiment and theoretical model.** Experimental modulations of the switching current I_S with the magnetic flux Φ piercing the SQUID at $T = 50$ mK for positive (a) and negative (b) current bias measured for positive values of voltage applied to the left gate electrode V_L . (c) Positive branch of $I_S(\Phi)$ for different negative values of V_L and for different values of positive right gate bias V_R (d) measured at $T = 50$ mK. In the experiment, the leakage current measured between the gate electrode and the SQUID is typically of the order of a few tens of pA resulting in a gate-SQUID impedance of a few T Ω . Theoretical modulations of I_S with Φ calculated with our RCSJ-based model for different values of current fluctuations and critical current suppression applied to the left (e) and right (f) JJ. The parameters used in the numerical simulations are listed in the Methods.

fluctuations are recorded for the second half period of $I_S(\Phi)$ oscillation. In addition, the values of V_R which are necessary to affect I_S are bigger than for V_L because the distance between the JJ and the gate electrode is larger in R than in L .

Our RCSJ-based model (see Methods for further details) allows to grasp the basic physics of the interferometer. Previous gating experiments performed on metallic JJs [2–4] suggest that the electric field can strongly reduce their switching current. We included this information in the model by reducing $I_{C,L}$ or $I_{C,R}$ (with $I_{C,L}$ and $I_{C,R}$ denoting the switching currents of the left and right JJ, respectively) when the corresponding gate bias is applied. In this case, a sizable screening parameter β is enough to explain both the reduction of the total switching current of the SQUID and the shift of the interference pattern along the magnetic flux axis [6, 18]. However, this is not sufficient to account for the difference in the switching current errors for the first and second half period of I_S (see Fig. 2-a). To this end, we introduced two gate-dependent fluctuating currents, $I_L^{\#}$ and $I_R^{\#}$, that disturb the dynamics of the corresponding superconducting phases. These are *local* noise sources exclusively acting on the left or right JJ due to the presence of the applied gate voltage, respectively. Yet, in the SQUID configuration the superconducting phases are locked by

fluxoid quantization [19]. Therefore, any local perturbation affects non-locally the dynamics of the opposite junction, and all the *global* observables of the interferometer. This will be a key point to explain some of the features of the following measurements.

Figures 2-e and f show the result of the calculation of the joint impact of the switching current reduction and phase fluctuations in the left and right JJ on the complete interference pattern of the SQUID, respectively. By imposing the phase noise on the left (right) JJ, the interference pattern shifts towards negative (positive) values of the magnetic flux, and the I_S fluctuations grow in the first (second) half of the switching current oscillation period. The theoretical curves display a good quantitative agreement with the experimental data. In particular, the calculations suggest that current fluctuations occur already for low values of gate voltage, while the critical current suppression start to develop for higher gate biases. As a consequence, our data seem to highlight that an external static electric field can affect, even if indirectly, the phase of a metallic conventional superconductor. We wish to stress that this result could not have been observed in previous experiments on single JJs [2–4], since only a phase-sensitive experiment, enabled by the SQUID geometry, is capable to shed light on this unconventional gating effect.

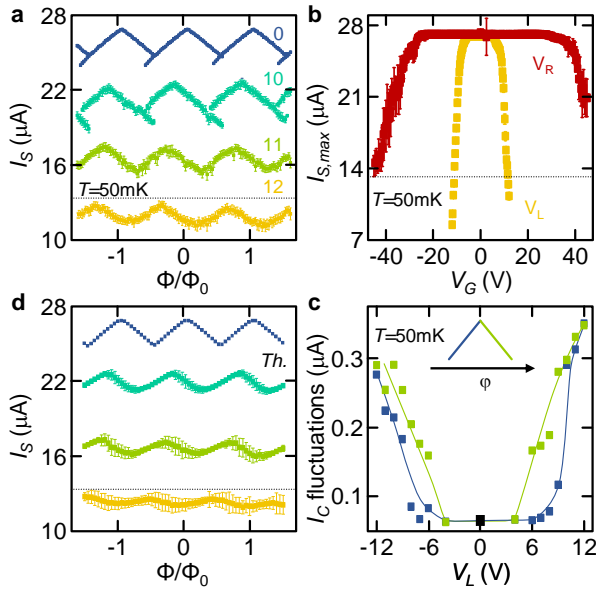


FIG. 3: **Impact of electric field on the superconducting phase.** **a** $I_S(\Phi)$ for different values of gate voltage V_L measured at $T = 50$ mK. The dotted black curve represents the intrinsic value of the critical current of the right JJ ($I_{C,R} \simeq 13.3 \mu\text{A}$). **b** Switching current for zero magnetic flux piercing the interferometer $I_{S,max}$ as a function of the bias voltage applied to left (yellow squares) and right (red squares) gate electrode at $T = 50$ mK. **c** Average fluctuations of SQUID switching current as a function of the bias applied to the left gate electrode V_L for the rising (blue squares) and decreasing (green squares) branch at $T = 50$ mK. **d** Switching current I_S as a function of the external magnetic flux Φ calculated within an *ad hoc* model based on the RCSJ formalism. In particular, we considered the joint impact of the dampening of the critical current $I_{C,L}$ of the left nano-constriction and the enhancement of the electric field-dependent superconducting current fluctuations I_L^{gate} on the same JJ. The parameters used in the numerical simulations are listed in the Methods.

Next step is to investigate the impact of the electrostatic field on the superconducting phase for higher values of gate voltage. Figure 3-a shows the experimental traces measured for $V_L \geq 10$ V at $T = 50$ mK. The most prominent feature is the suppression of I_S below the critical current of a single JJ for every value of the magnetic flux [$I_S(V_L = 12\text{V}) \leq I_{C,R}$, see black dotted line in Fig. 3-a], while the oscillatory behavior is preserved with an almost constant visibility. The stark reduction of the switching current is highlighted by plotting $I_{S,max} = I_S(\Phi = 0)$ as a function of gate voltage (see Figure 3-b). In particular, for $V_L = -12$ V the switching current surprisingly lowers down to $\sim 0.6I_{C,R}$. Furthermore, the asymmetry in the switching current fluctuations for the first/second half of the oscillation period of $I_S(\Phi)$ tends to disappear for high values of gate bias (see Figure 3-c). In addition, the multivalued nature of I_S for

certain values of Φ turns out to vanish by increasing gate voltage.

All the above phenomenology does not find any satisfactory explanation within conventional models for a SQUID [6, 18] with the assumption that the junction critical current decreases under the effect of the electric field [1–4] or for a possible direct hot electron injection [20]. In fact, if a single JJ is squeezed up to closure, a continuous and flux-independent flow of current in the ungated junction is expected to occur [6]. By contrast, Figs. 3-a and b imply that a local static electric field (see Fig. 1-e) influences both junctions thereby affecting the whole interferometer. Our theoretical model appears to reconcile all these observations. In particular, it seems to be able to account for both the strong I_S decrease and the symmetrization of its fluctuations (see Fig. 3-c).

Figure 3-d shows the evolution of $I_S(\Phi)$ calculated by imposing, on the one hand, the dampening of the critical current $I_{C,L}$ of the left JJ and, on the other hand, the strengthening of the gate-dependent current fluctuations on the same junction I_L^{B} . As discussed above, owing to fluxoid quantization, the local noise I_L^{B} actually perturbs the dynamics of the superconducting phase of the right junction leading eventually to suppression of I_S below the value of the ungated junction (Fig. 3-d). The theoretical curves exhibit a good qualitative agreement with the experiment. In addition, they are able to grab the evolution from a triangular-shaped interference pattern of $I_S(\Phi)$ to a smoother oscillatory behavior. We can therefore conclude that an external electrostatic field *couples* with the superconducting phase of a conventional metallic superconductor.

The sliding of the interference pattern along the magnetic flux axis driven by the gate bias can be inherently projected in a tunable shift of the superconducting phase [6]. We define the phase shift as $\Delta\varphi(V_i) = \varphi(V_i) - \varphi(0)$, where V_i is the voltage applied to the $i = L, R$ gate electrode. Figure 4-a shows the phase shift as a function of V_L (yellow squares) and V_R (red squares) extrapolated from our experimental data obtained at $T = 50$ mK. Notably, the total maximum phase shift is $\Delta\varphi_{\text{tot}} = \Delta\varphi_{\text{max}}(V_R) - \Delta\varphi_{\text{max}}(V_L) \simeq 0.6\pi$, where $\Delta\varphi_{\text{max}}(V)$, with $V = V_R, V_L$, is the maximum phase shift generated by applying the voltage V . The asymmetry in the effect of the two gate voltages on $\Delta\varphi$ can be entirely ascribed to the difference in the distance of the two gate electrodes from the corresponding weak-link regions [3]. From our data we can extrapolate a possible total maximum phase shift of at least 0.8π within this geometry, since a $\Delta\varphi \sim 0.4\pi$ was obtained by biasing the left gate electrode (see Fig. 4-a). In addition, we wish to stress that the maximum achievable phase shift could rise by applying stronger gate biases until the oscillatory behavior of $I_S(\Phi)$ is preserved.

The dependence of the switching current interference pattern on temperature provides important information

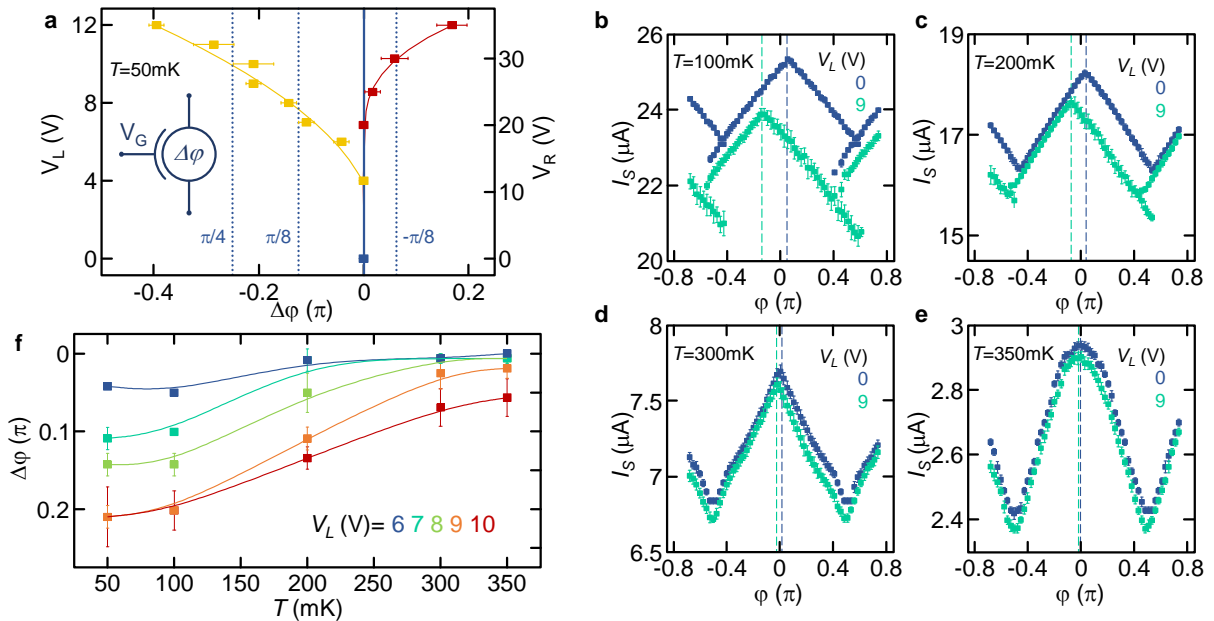


FIG. 4: **Phase shift and its temperature dependence.** **a** Phase shift $\Delta\varphi$ as a function of the voltage applied to left (yellow squares) and right (red squares) gate electrode at $T = 50$ mK. Dashed lines indicate typical phase shifts required for implementing quantum logic gates: $\pi/8$ and $\pi/4$ (the so-called T gate). The inset shows the schematic representation of a gate-tunable phase shifter. **b-e** Modulations of the switching current I_C with the superconducting phase φ measured at four different temperatures $T = 100, 200, 300, 350$ mK for two values of V_L (0, blue squares, and 9 V, turquoise squares). The dashed lines represent the phase position of $I_{C,max}$ for $V_L = 0$ (blue) and $V_L = 9$ V (turquoise). **f** Phase shift $\Delta\varphi$ as a function of temperature for different values of the voltage applied to the left gate electrode V_L . The squares depict the averages of $\Delta\varphi$ extracted from different periods with the associated error, while the solid lines are guides for the eye.

about the impact of the electric field on the Josephson coupling and on the efficiency of the phase shifter. In particular, Figs. 4-b-e show the evolution of the ungated $I_S(\varphi)$ traces (blue squares) with temperature. On the one hand, the transition from a linear to a smooth trace is related to the current-phase relation of the JJs approaching the conventional sinusoidal behavior by increasing the temperature [15, 16]. On the other hand, the disappearance of a multivalued $I_S(\Phi)$ is related to the decrease of the screening parameter [17]. The latter, together with a lower impact of the electric field on the supercurrent [1–3], is also reflected in the decrease of the phase shift caused by $V_L = 9$ V at higher temperatures (see Figs. 4-b-e).

The full behavior of $\Delta\varphi$ on temperature for different values of gate bias applied to the left JJ is summarized in Fig. 4-f. The phase shift decreases monotonically by increasing T for all the applied values of gate voltage. However, the phase shift persists up to about 85% of T_C for $V_L \geq 8$ V denoting a wide range of operating temperatures.

Beyond the strong implications in fundamental physics, i.e., the apparent coupling of a static electric field to the macroscopic phase of the superconducting condensate, gate-controllable metallic Josephson interferometers may be the cornerstone for several supercon-

ducting field-effect devices with a wide range of possible applications. For instance, the possibility to manipulate and change the interferometric phase can yield important implications in quantum information [10, 11] in the form of flux [12, 25] and phase [26] superconducting qubits, and in superconducting electronics [8] for the realization of electrostatically-tunable rapid single flux quantum (RSFQ) logic [27]. Furthermore, the ability of electrostatically mastering $I_S(\Phi)$ could be of fundamental importance for the implementation of ultrasensitive tunable magnetometers [13, 14]. Finally, these prototypical interferometers could find application in phase-controllable caloritronics [28, 29] and single photon sensing [30].

Methods

Fabrication

The samples were nano-fabricated by single step electron-beam lithography and evaporation of Ti through a poly(methyl methacrylate) (PMMA) mask onto an intrinsic Si wafer covered by 300 nm of silicon dioxide. The 30 nm thick Ti film was deposited at room temperature in an ultrahigh-vacuum electron-beam evaporator with a

base pressure of about 5×10^{-11} torr at a rate of about 11 Å/s.

Measurements

All measurements were performed in a filtered He³-He⁴ dry dilution refrigerator at different bath temperatures in the range 50mK - 450mK using standard four-wire technique. The resistance versus temperature characteristics were obtained by low frequency lock-in technique. To this end, a.c. excitation currents with typical root mean square amplitudes $I \simeq 10$ nA at a frequency of 13.33 Hz were imposed through the device. The magnetic-flux patterns of the devices were obtained by injecting a low-noise biasing current and measuring the voltage drop by a room-temperature differential preamplifier. The gate bias was applied by a low-noise high-input impedance source/measure unit. Every measurement point is the average over 50 repetitions and the respective error is their standard deviation.

Finite element simulations

The three-dimensional finite element method calculations of the intensity of the electric displacement vector \vec{D} was performed by solving the Gauss' law $\vec{\nabla} \cdot \vec{D} = 0$ for the same geometry of the field-effect controllable interferometer. In our calculation the gate electrodes and the SQUID were approximated as ideal conductor boundaries with the constrains of $V_L = 1$ V on the gate surfaces, $V = 0$ on the SQUID and the right gate is kept floating (as in the experiments). Since the structure of the device is fully symmetric, by applying the bias to the right gate electrode we would obtain the same result.

Theoretical model

The operation of a SQUID based on Dayem bridges can be determined by solving the system of resistively and capacitively shunted junction (RCSJ) equations [21]:

$$\frac{I}{2} + I_{circ} + I_L^h + I_L^{\mathbf{B}} = \frac{\hbar}{2e} C_L \ddot{\varphi}_L + \frac{\hbar}{2e} \frac{1}{R_L} \dot{\varphi}_L + I_L(\varphi_L) \quad (1)$$

$$\frac{I}{2} - I_{circ} + I_R^h + I_R^{\mathbf{B}} = \frac{\hbar}{2e} C_R \ddot{\varphi}_R + \frac{\hbar}{2e} \frac{1}{R_R} \dot{\varphi}_R + I_R(\varphi_R), \quad (2)$$

where I is the external bias current, I_{circ} is the current circulating in the superconducting ring, and e is the electron charge. Moreover, C_i , R_i , I_i , and φ_i are the capacitance, the normal-state resistance, the Josephson current, and the phase difference of the i -th JJ (with $i = L, R$), respectively.

In Eqs. (1)-(2), the JohnsonNyquist noise terms, I_L^h and I_R^h , take into account the effect of temperature fluctuations on the phase dynamics and can be characterized by the relations [18]:

$$\langle I_i^h(t) \rangle = 0 \quad \langle I_i^h(t) I_i^h(t') \rangle = 2 \frac{k_B T}{R_i} \delta(t - t'). \quad (3)$$

Additionally, we enriched the numerical model with two gate-dependent Gaussianly-distributed, delta-correlated stochastic noise fluctuations, $I_i^{\mathbf{B}}$, with intensity $D_i^{\mathbf{B}}$, so that

$$\langle I_i^{\mathbf{B}}(t) \rangle = 0 \\ \langle I_i^{\mathbf{B}}(t) I_i^{\mathbf{B}}(t') \rangle = D_i^{\mathbf{B}} \delta(t - t'). \quad (4)$$

We approximate the CPR of the Josephson junctions with the non-sinusoidal Kulik-Omel'Yanchuk CPR for diffusive junctions KO-1 [22]:

$$I_i(\varphi_i) = \frac{\pi \Delta_i}{e R_i} \cos\left(\frac{\varphi_i}{2}\right) \tanh^{-1} \left[\sin\left(\frac{\varphi_i}{2}\right) \right], \quad (5)$$

where Δ_i is a BCS superconducting gap. Then, the critical current of each Josephson junction can be expressed as:

$$I_{c,i} = \max_{\varphi} I_i(\varphi) \simeq \frac{2\pi \Delta_i}{3e R_i}. \quad (6)$$

The numerical solution of Eqs. (1)-(2) demands the imposition of flux quantization in a superconducting ring interspersed with two weak links, that can be expressed as:

$$\varphi_L - \varphi_R = 2\pi \frac{\Phi}{\Phi_0} - \beta \frac{I_{circ}}{\bar{I}_C} + 2\pi k. \quad (7)$$

Here, Φ is the external magnetic flux, k is the number of enclosed flux quanta in the ring, $\bar{I}_C = (I_{C,L} + I_{C,R})/2$, while β is the screening parameter defined as

$$\beta = \frac{2\pi L}{\Phi_0} \bar{I}_C, \quad (8)$$

with L being the total inductance of the superconducting ring. The flux generated by I_{circ} tends to screen the applied flux Φ , according to the Faraday-Lenz law.

Finally, we observe that for the device shown in Fig.1 we can reasonably neglect any geometrical asymmetry in the SQUID inductance. This means that, in the ungated case, we can impose $L_1 = L_2 = L/2$, with L_1 and L_2 being the inductances of the left and right arms of the SQUID, respectively. Nonetheless, due to the closeness of the gating electrode to the superconducting leads forming each JJ, see the inset of Fig. 1-e, we can also expect that an applied voltage could slightly affect the

kinetic inductance of a SQUID arm. Specifically, we assume in our model that a gate voltage applied on the left (right) JJ increases the kinetic inductance of the left (right) SQUID arm, so that the i -th gated inductance becomes $L_i^{\#} = \alpha_\ell(V_i)L_i = \alpha_\ell L/2$, with $i = L, R$ and $\alpha_\ell(V_i) \geq 1$ (specifically, in the ungated case $\alpha_\ell = 1$). Consequently, Eq. (7) can be recast in [6]

$$\varphi_L - \varphi_R = 2\pi \frac{\Phi}{\Phi_0} - \beta \frac{\alpha_\ell + 1}{2} \frac{I_{circ}}{I_c} \pm \beta \frac{\alpha_\ell - 1}{2} \frac{I_b}{2I_c} + 2\pi k, \quad (9)$$

where the sign of the additional term depends on which junction the gate voltage is applied. By slightly increasing the inductance of a SQUID arm we observe two distinct phenomena. First, the shift from zero of the I_c maximum changes, since it can be estimated as $2\pi \frac{\Delta\Phi}{\Phi_0} = \beta(\alpha_I + \alpha_L)$ [6], where the asymmetry parameters read $\alpha_I = \frac{I_{C,L} - I_{C,R}}{I_{C,L} + I_{C,R}}$ and $\alpha_L = \frac{L_L - L_R}{L_L + L_R}$. Specifically, by assuming to perturb the left junction, we obtain $\Delta\Phi = L(\alpha_\ell I_{C,L} - I_{C,R})/2$. Moreover, for $\beta \gg 1$ it can be shown that $\Delta I_c / I_{C,max} \sim \pi/\beta$ [6], that is $\Delta I_c \sim \Phi_0 / (L_L + L_R)$. Then, the higher the inductance of a SQUID arm, the lower the modulation ΔI_c of the critical current patterns.

The solution of Eqs. (1)-(2) can be dealt along the lines of the numerical approach developed in Refs. [23, 24]. Then, the switching current of the SQUID is obtained by slowly, linearly ramping the bias current I_b , and recording the value at which a non-negligible mean voltage drop appears. Thus, the repetition of this stochastic process allows to calculate the fluctuations in the SQUID switching current. Finally, each I_c pattern is obtained by taking, at a fixed Φ , the maximum switching currents between that ones calculated by changing the number k of enclosed flux quanta in the ring. Therefore, this method does not allow to catch the bistability shown by experimental data.

With the aim to obtain numerically critical current patterns that approximate the experimental curves well, we impose the parameter values listed below

V_L (V)	$I_{C,L}$ (μ A)	$\alpha_{L,R}^{\text{gate}}$	α_ℓ
0	13.6	0	0
7	13.6	7	0
8	13.6	8	0
9	13.6	14	1.05
10	12	19	1.17
11	9.5	30	1.23
12	7.5	45	1.28
V_R (V)	$I_{C,R}$ (μ A)	$\alpha_{L,R}^{\text{gate}}$	α_ℓ
30	13.3	4	0
35	13.3	7.5	0

where the coefficient $\alpha_{L,R}^{\#}$ makes possible to express the intensity of the additional noise source in terms of the intensity of the thermal fluctuations, namely, $D_i^{\#} = \alpha_i^{\#} \times D_i^{\text{h}}$ where $D_i^{\text{h}} = \sqrt{2k_B T / R_i}$ with $i = L, R$.

Lastly, the capacitances of the junctions were set at $C_1 = C_2 = 10$ fF, while the normal-state resistances estimated from the ungated critical current pattern read $R_L \simeq 10.5 \Omega$ and $R_R \simeq 10.7 \Omega$.

* Electronic address: federico.paolucci@pi.infn.it

† Electronic address: francesco.giazotto@sns.it

- [1] De Simoni, G., Paolucci, F., Solinas, P., Strambini, E. & Giazotto, F. Metallic supercurrent field-effect transistor, *Nat. Nanotech.* **13**, 802, 2018.
- [2] Paolucci, F., De Simoni, G., Strambini, E., Solinas, P. & Giazotto, F. Ultra-Efficient Superconducting Dayem Bridge Field-Effect Transistor, *Nano Lett.* **18**, 4195, 2018.
- [3] Paolucci, F., De Simoni, G., Solinas, P., Strambini, E., Ligato, N., Virtanen, P., Braggio, A. & Giazotto, F. Magnetotransport Experiments on Fully Metallic Superconducting Dayem-Bridge Field-Effect Transistors, *Phys. Rev. Appl.* **11**, 024061, 2019.
- [4] De Simoni, G., Paolucci, F., Puglia, C. & Giazotto, F. Mesoscopic Al/Cu/Al Josephson field-effect transistors, *arXiv:1903.03435*, , 2019.
- [5] Virtanen, P., Braggio, A. & Giazotto, F. Superconducting size effect in thin films under electric field: mean-field self-consistent model, *arXiv:1903.01155*, , 2019.
- [6] Clarke, J. & Braginski, A. *The SQUID Handbook: Fundamentals and Technology of SQUIDs and SQUID Systems* (Wiley, 2004).
- [7] Clark, T. D., Prance, R. J. & Grassie, A. D. C. Feasibility of hybrid Josephson field effect transistors, *J. Appl. Phys.* **51**, 2736, 1980.
- [8] Terzioglu, E., & Beasley, M. R. Complementary Josephson junction devices and circuits: a possible new approach to superconducting electronics, *IEEE Trans. Appl. Supercond.* **8**, 48, 1998.
- [9] Devoret, M. H. & Schoelkopf, R. J. Superconducting Circuits for Quantum Information: An Outlook, *Science* **339**, 1169, 2013.
- [10] Majer, J. B., Butcher, J. R. & Mooij, J. E. Simple phase bias for superconducting circuits, *Appl. Phys. Lett.* **80**, 3638, 2002.
- [11] Ioffe, L. B., Geshkenbein, V. B., Fiegel'man, M. V., Fauchere, A. L., & Blatter, G. Environmentally decoupled sds-wave Josephson junctions for quantum computing, *Nature* **398**, 670, 1999.
- [12] Mooij, J. E., Orlando, T. P., Levitov, L., Tian, L., van der Wal, C. H. & Lloyd, S. Josephson Persistent-Current Qubit, *Science* **285**, 1036, 1999.
- [13] Anahory, Y., Reiner, J., Embon, L., Halbertal, D., Yakovenko, A., Myasoedov, Y., Rappaport, M. L., Huber, M. E. & Zeldov, E. Three-Junction SQUID-on-Tip with Tunable In-Plane and Out-of-Plane Magnetic Field Sensitivity, *Nano Lett.* **14**, 6481, 2014.
- [14] Uri, A., Meltzer, A. Y., Anahory, Y., Embon, L., Lachman, E. O., Halbertal, D., Naren, HR., Myasoedov, Y., Huber, M. E., Young, A. F. & Zeldov, E. Electrically Tunable Multiterminal SQUID-on-Tip, *Nano Lett.* **14**, 6481, 2014.
- [15] Fulton, T. A., Dunkleberger, L. N. & Dynes, R. C. Quantum Interference Properties of Double Josephson Junctions

- tions, *Phys. Rev. B* **6**, 855, 1972.
- [16] Tsang, W.-T. & Van Duzer, T dc analysis of parallel arrays of two and three Josephson junctions, *J. Appl. Phys.* **46**, 4573, 1975.
- [17] Russo, R., Granata, C., Vettoliere, A., Esposito, E., Fretto, M., De Leo, N., Enrico, E. & Lacquaniti, V. Performances of niobium planar nanointerferometers as a function of the temperature: a comparative study, *Supercond. Sci. Technol.* **27**, 044028, 2014.
- [18] Barone, A. & Paternò, G. *Physics and Applications of the Josephson Effect* (Wiley, 1982).
- [19] Tinkham, M. *Introduction to Superconductivity* (McGraw-Hill, 1996).
- [20] Morpurgo, A., Klapwijk, T. M. & van Wees, B. J. Hot electron tunable supercurrent, *Appl. Phys. Lett.* **72**, 966, 1998.
- [21] Granata, C. & Vettoliere, A. Nano Superconducting Quantum Interference device: A powerful tool for nanoscale investigations, *Phys. Rep.* **614**, 1, 2016.
- [22] Kulik, I. & Omel'Yanchuk, A. Contribution to the microscopic theory of the Josephson effect in superconducting bridges, *Sov. J. Exp. Theor. Phys. Lett.* **21**, 96, 1975.
- [23] Solinas, P., Gasparinetti, S., Golubev, D. & Giazotto, F. A Josephson radiation comb generator, *Sci. Rep.* **5**, 12260, 2015.
- [24] Guarcello, C., Solinas, P., Braggio, A., Di Ventura, M. & Giazotto, F. Josephson Thermal Memory, *Phys. Rev. Applied* **9**, 014021, 2018.
- [25] Yan, F., et al., The flux qubit revisited to enhance coherence and reproducibility, *Nat. Commun.* **7**, 12964, 2016.
- [26] Martinis, J. M., Nam, S., Aumentado, J. & Urbina, C. Rabi Oscillations in a Large Josephson-Junction Qubit, *Phys. Rev. Lett.* **89**, 117901, 2002.
- [27] Likharev, K. K. & Semenov, V. K. RSFQ logic/memory family: a new Josephson-junction technology for sub-terahertz-clock-frequency digital systems, *IEEE Trans. Appl. Supercond.* **1**, 3, 1991.
- [28] Fornieri, A. & Giazotto, F. Towards phase-coherent caloritronics in superconducting circuits, *Nat. Nanotech.* **12**, 944, 2017.
- [29] Giazotto, F., Robinson, J. W. A., Moodera, J. S. & Bergeret, F. S. Proposal for a phase-coherent thermoelectric transistor, *Appl. Phys. Lett* **105**, 062602, 2014.
- [30] Virtanen, P., Ronzani, A. & Giazotto, F. Josephson Pho-

todetectors via Temperature-to-Phase Conversion, *Phys. Rev. Applied* **9**, 054027, 2018.

Acknowledgements

We acknowledge F. S. Bergeret, A. Braggio, V. Golovach, E. Strambini, S. Kafanov, A. Romito and Y. Pashkin for fruitful discussions.

The authors acknowledge the European Research Council under the European Union's Seventh Framework Programme (COMANCHE; European Research Council Grant No. 615187) and Horizon 2020 and innovation programme under grant agreement No. 800923-SUPERTEd. The work of G.D.S. and F.P. was partially funded by the Tuscany Region under the FARFAS 2014 project SCIADRO. The work of F.P. was partially supported by the Tuscany Government (Grant No. POR FSE 2014-2020) through the INFN-RT2 172800 project.

Author contributions statement

F.P. fabricated the samples. F.P., F.V. and G.D.S. performed the measurements. F.P. and F.V. analysed the experimental data with input from G.D.S. and F.G.. C.G. developed the theoretical model with inputs from F.G. and P.S.. G.D.S. performed the finite element simulations. F.G. conceived the experiment. F.P. wrote the manuscript with input from all authors. All authors discussed the results and their implications equally at all stages.

Additional information

The authors declare no competing financial interests.